Contrasting dynamics of past climate states and critical transitions via dimensional analysis

Tommaso Alberti, Fabio Florindo, Eelco J Rohling, Valerio Lucarini, Davide Faranda

Contrasting dynamics of past climate states and critical transitions via dimensional analysis

Tommaso Alberti[1*], Fabio Florindo[1], Eelco J. Rohling[2], Valerio Lucarini[3,4], Davide Faranda[5,6,7]

[1]Istituto Nazionale di Geofisica e Vulcanologia, via di Vigna Murata 605, Rome, 00143, Italy.
[2]School of Ocean and Earth Science, University of Southampton, Southampton, SO14 3ZH, UK.
[3]University of Leicester, Leicester UK.
[4]Centre for the Mathematics of Planet Earth, University of Reading, Reading, RG6 6AX, UK.
[5]Laboratoire des Sciences du Climat et de l'Environnement, CEA Saclay l'Orme des Merisiers, UMR 8212 CEA-CNRS-UVSQ, Gif-sur-Yvette, 91191, France.
[6]London Mathematical Laboratory, 8 Margravine Gardens, London, W6 8RH, UK.
[7]Laboratoire de Météorologie Dynamique/IPSL, École Normale Supérieure, PSL Research University, Sorbonne Université, 75005, Paris, France, École Polytechnique, IP Paris, Paris, 75005, France.

*Corresponding author(s). E-mail(s): tommaso.alberti@ingv.it;
Contributing authors: fabio.florindo@ingv.it; eelco.rohling@anu.edu.au; v.lucarini@leicester.ac.uk; davide.faranda@lsce.ipsl.fr;

Abstract

While past major climate transitions can be unequivocally identified, understanding of underlying mechanisms and timescales is lacking. We employ a dimensional analysis of benthic stable isotope records across different timescales to uncover how Cenozoic climatic fluctuations are associated with changes in the number of feedbacks and mechanisms involved. Our analysis indicates that warmer and colder climates respond substantially differently to orbital forcing. Notably, a that large numbers of feedbacks dominated during the Icehouse state at obliquity and eccentricity timescale, and during the Warmhouse and Hothouse states

at precession timescales. During the Coolhouse state the number of active feedbacks was low and had no dominant timescale. Coupling between climate signals that affect oxygen and carbon isotope records appears high only in the Icehouse state, and low to absent in all other states. We also find that anomalously high active feedback numbers and very high coupling occurred across all timescales during the PETM, which suggests a complete system perturbation. In conclusion, our findings challenge the notion of a singular model of interconnected feedbacks in reproducing Cenozoic paleoclimate variability, given that different numbers of active feedbacks with different levels of coupling governed over different timescales between climate states, which then affected the inherent (in-)stability of each climate state.

Keywords: Cenozoic climate variability, Abrupt climate shifts, Dimensional analysis

1 Introduction

Earth's climatic history has been reconstructed using sediment archives from both marine and terrestrial environments. In particular, the development of high-resolution deep-sea oxygen (δ^{18}O) and carbon (δ^{13}C) isotope records has since the 1970s [1, 2] greatly enhanced understanding of past climate trends, cyclic variations, rates of change, and transient events throughout the Cenozoic era (66 My ago to present). However, the compilations have suffered limitations in accurately documenting the full range and detailed characteristics of Cenozoic climate variability, due to gaps and insufficient age control and temporal resolution, especially for the period before 34 My ago. A recent study [3] addressed these challenges by utilizing sediment archives obtained by the International Ocean Discovery Program (IODP) and its predecessor programs (DSDP, ODP) to compile and analyze a comprehensive new composite record of carbon and oxygen isotopes in deep-sea benthic foraminifera that was precisely tuned to astronomical cycles. The new climate reference curve, CENOGRID (CENOzoic Global Reference benthic foraminiferal carbon and oxygen Isotope Dataset) [3], provides high-resolution coverage of the past 66 My to detect long-term Cenozoic climate variability (Figure 2A).

Employing statistical recurrence analysis (RA) on the CENOGRID record, Westerhold et al. [3] identified four key climatic regimes in the Cenozoic era: Hothouse, Warmhouse, Coolhouse, and Icehouse, each demonstrating unique and statistically significant dynamics [3]. The Warmhouse and Hothouse states prevailed from approximately 66 million years ago (the Cretaceous/Paleogene boundary) to about 34 million years ago (the Eocene-Oligocene Transition). During these periods, temperatures exceeded present-day levels by more than $\geq$5°C and $\geq$10°C, respectively. Notably, the Hothouse climate state witnessed transient warming events known as hyperthermals, marked by concurrent negative excursions in δ^{13}C and δ^{18}O, indicating substantial carbon release into the climate system and global warming [4–8].

The Warmhouse-Coolhouse transition occurred at the Eocene-Oligocene Transition, accompanied by a significant temperature drop and establishment of a

semi-permanent Antarctic Ice Sheet [8–12]. The Coolhouse state extended from approximately 34 million years ago to 3.3 million years ago and comprised two phases, separated around 14 million years ago by a δ^{18}O increase and transient δ^{13}C rise in the deep ocean, signaling rapid Antarctic Ice Sheet expansion [13, 14]. The Icehouse state, characterized by the fluctuation of ice sheets in the Northern Hemisphere, was fully established during the Pliocene-Pleistocene transition [15] and continues until the present.

The Cenozoic climate has experienced several transitions [3, 16] associated with tipping points [17] of the Earth system. In Ref. [18] such transitions have been characterized, by combining recurrence analysis of the individual time series [19, 20] with a multi-variate analysis based on the quasi-potential theory [21, 22]. In addition to the critical transitions between the four macroclusters of climate variability mentioned above, the analysis identified several other occurrences of tipping behaviour [18].

Here we aim to offer a further advance by applying a multiscale and bivariate dimensional analysis of the CENOGRID record [23, 24] to rank and characterize the four climate states in terms of number of effective feedback and associated timescales, together with stability/predictability in the record with a focus on the critical transitions, and δ^{13}C-δ^{18}O coupling at multi-millennial timescales (see schematic in Figure 1).

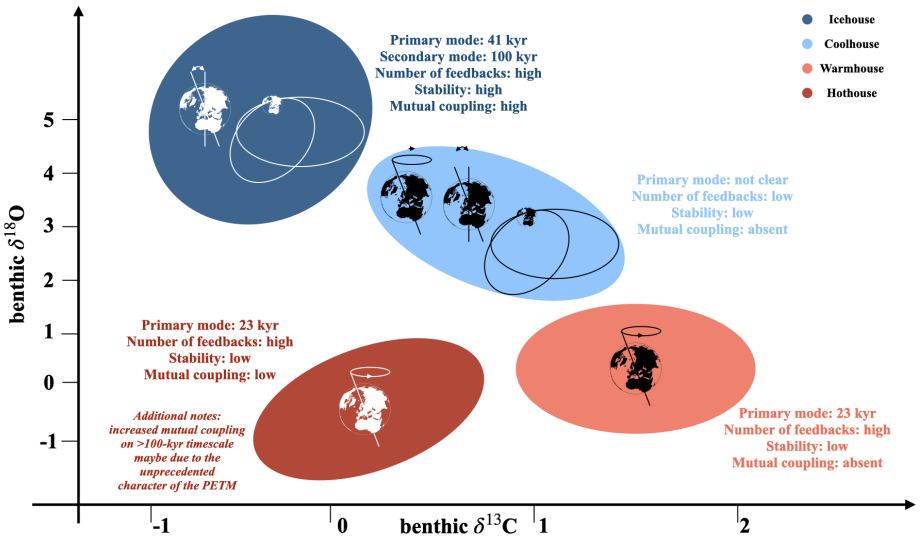

Fig. 1 Schematic of the main features of the four main climate states. The four climate states are ranked in terms of number and timescales of effective feedbacks, stability/predictability, and δ^{13}C-δ^{18}O coupling at multi-millennial timescales.

So far, this type of analysis has proved great skills in other different applications [23, 24]. In our application, it extracts intrinsic scale-dependent components from the CENOGRID δ^{13}C and δ^{18}O records via Empirical Mode Decomposition (EMD) [25]

and determines, across timescales (τ), three key parameters [26–28]: (1) instantaneous dimension d, which provides an estimate of the number of positive feedbacks (more mechanisms acting on the system lead to higher than average values of d); (2) extremal index θ, which quantifies the stability with respect to perturbations of the system; i.e., its intrinsic persistence, where θ close to 0 (1) means that the system persists for longer (shorter) in a given state; and (3) co-recurrence ratio α, which quantifies the mutual coupling between two proxies, with α close to 1 (0) meaning stronger (weaker) coupling. It is well known that, depending on the timescale of interest, the same system might exhibit different stability properties, depending on whether positive or negative feedbacks dominate [29]. We note that the instantaneous dimension should be interpreted in relative rather than absolute terms. Rather than taking the obtained estimate of d at face value, we proceed as follows. If, e.g., state (a) features a larger d value than state (b), then we conclude that the number of effective feedback mechanisms of state (a) is larger. Furthermore, if, e.g., state (c) features a larger value of d at the timescale τ_1 than at timescale τ_2, then we rank τ_1 as the primary/dominant mode of variability. Key aspects of the EMD, an in-depth description of the uni-variate and bi-variate parameters, and our scale-dependent procedure are reported in the Methods.

Multiscale analysis of the CENOGRID dataset

The behavior of our multiscale bivariate metrics (Figure 2) highlights key properties of the climate variability recorded in the CENOGRID dataset. The instantaneous dimension d (Figure 2A) clearly indicates a lower number of effective feedback during the Coolhouse than during the other climate states, except for an increase during specific events such as the Monterey positive carbon isotope excursion between 16.9 and 13.5 My ago [30] that lacks dominant expression of any specific orbital period. The timescale-dependent estimate of d reveals that, while the Warmhouse and the Hothouse states are dominated by active positive feedbacks (larger d) at short orbital timescales (mainly precession), the Icehouse is dominated by active positive feedbacks at obliquity and eccentricity timescales. For warm climates this can be due to the moderate-to-high carbon dioxide levels and the existence of a mix of tropical and temperate ecosystems observed during both the Hothouse and the Warmhouse, which is also evident from the uni-variate analysis (Supplementary Figures S1-S2) which shows larger d for the δ^{13}C than δ^{18}O. Conversely, for the Icehouse this can be related to the presence of enhanced polar ice sheets and glaciers, enhancing ice-ocean-atmosphere coupling processes, and associated greenhouse gas variability. In general, we observe substantial short-term ($\tau \lesssim 23$ ky) mutual coupling (increased α; Figure 2D) between δ^{13}C and δ^{18}O during warm climate states, especially after the PETM, which no longer occurs during cold climate states, together with temporarily strongly enhanced coupling during specific intervals such as the Late Danian, Early Eocene Hyperthermals, and the middle Miocene Monterey event. During the Icehouse, starting from the M2 glaciation, prolonged mutual coupling is found at obliquity and eccentricity timescales, which did not persistently occur before. This is related to the repeated glacial-interglacial variations, whereby a strong coupling is established between the

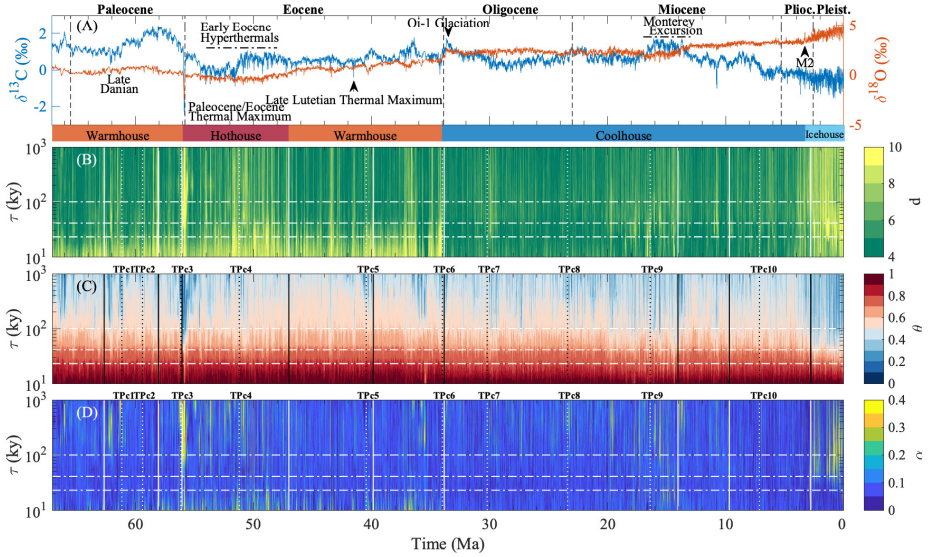

Fig. 2 Multiscale bivariate analysis during the last 66 Ma. (A) Time series of the CENOGRID paleoclimate records of $\delta^{13}C$ (blue) and $\delta^{18}O$ (red) during the last 66 Ma. Bi-variate multi-scale metrics: (B) instantaneous dimension d, (C) extremal index θ, and (D) co-recurrence index α. Vertical dashed lines in panel (A) mark the different geological epochs, while specific events are reported when they occurred. Vertical continuous and dotted lines in panels (B)-(D) indicate the Tipping Points (TPs) identified by Rousseau et al. [18] with a uni-variate approach for δ^{18}O and δ^{13}C, respectively. The horizontal dashed-dotted white lines refer to Milankovitch timescales of precession ($\sim$ 23 ky), obliquity ($\sim$ 41 ky), and eccentricity ($\sim$ 100 ky), respectively. We note that θ close to 0 (1) means a more (less) stable/persistent state, while α close to 0 (1) means a less (more) mutual coupling.

average surface temperature and the intensity of the carbon cycle. Furthermore, while all climate states are characterized by low-stability behavior (high θ; Figure 2C) at timescales shorter than the obliquity period, increased stability/persistence (lower θ) is observed at obliquity and eccentricity timescales during the Icehouse climate state, marking the current climate state as the one with most persistent responses at orbital 41- and 100-ky timescales out of the entire past 66 My, related to the glacial-interglacial cycles.

Finally, our analysis uniquely highlights the exceptional nature, even among other hyperthermals, of the Paleocene Eocene Thermal Maximum (PETM), where d is high and almost constant across all timescales and lacks association with any particular orbital timescale, while coupling is high at all timescales (high α; Figure 2C). In contrast, the Eocene-Oligocene Transition (EOT, $\sim$34 Ma) seems to be primarily influenced by processes at precession timescales, marking the end of the precession-dominated Hot-/Warmhouse period. Both these transitions were identified recently as key abrupt transitions (Tipping Points, TPs) associated with major regime shifts that separate clusters of climate variability [18], although here we also provide a rank in terms of active feedback and associated timescales.

Dynamical Features of the Four Climate Variability Macroclusters across Timescales

To facilitate interpretation of our results, we investigate the average values of d, θ, and α in the timescale domain (τ) for the four climate states as compared with those of the full record (Fig. 3).

The Hothouse climate state is characterized by d decrease with increasing τ, with a bit of a plateau around the 100-ky eccentricity period, which indicates the largest number of feedbacks in the climate response at around the 23-ky precession timescale. Thus, the primary mode of variability of the Hothouse climate is recognized to be precession. A similarly decreasing trend with τ is visible for θ, which suggests increased climate stability at the primary mode (precession) of variability. Finally, α is clearly high at precession timescales, as well as at timescales larger than the eccentricity period. The former can be related to responses to precession variations, but the latter mainly is due to the PETM signature. The Warmhouse state is also characterized by decreasing d and θ with increasing τ, while d values are lower and θ values similar, relative to the Hothouse. As opposed to the Hothouse, the Warmhouse is characterized by approximately constant α for all timescales at around 0.1, which indicates low mutual coupling between δ^{13}C-δ^{18}O. Based on the d behavior we identify precession as the primary mode of variability.

During the Coolhouse state, a different behavior is observed, characterized by absence of a clearly dominant timescale for d. Yet, θ and α decrease with τ in a similar manner as observed in the warm climate states, and values are also similar to those in the warm states. This decrease in θ and α metrics reflects relatively stable conditions during the Coolhouse state. Based on the timescale-independence of d we are not able to find a primary mode of variability for the Coolhouse. Finally, results differ completely for the Icehouse state, with a high overall number and slight timescale-dependence for d, which peaks at around the 41-ky obliquity timescale, reaching a plateau around the 100-ky eccentricity timescale. This suggests an increased number of feedback mechanisms involved in climate responses at both 41- and 100-ky timescales, relative to the prior warm climate states and the Coolhouse state (centered on the 23-ky timescale). Thus, we rank the obliquity and the eccentricity cycles as the primary and secondary modes of variability, respectively. Meanwhile, extremal index θ, while still characterized by a decrease with τ, shows considerably lower values (i.e., greater stability since θ approaches 0) than the previous climate states. Additionally, α is once again highly timescale dependent, but now peaks at 41 and 100 ky timescales, reaching higher values than previously observed. This behavior likely reflects an increse in ice-ocean-atmosphere interactions.

Overall, our analysis implies that warmer and colder climates respond substantially differently to orbital forcing. Responses during warm climates are dominated by precession timescale variations, whereas cold climates appear to be driven mainly by responses on obliquity and eccentricity timescales.

To further inspect climate responses at orbital timescales, we investigate the 2-D (d, θ) parameter-space behavior and the probability distribution functions (pdfs) in the four climate states (Fig. 4), as well as in different geological epochs (Supplementary

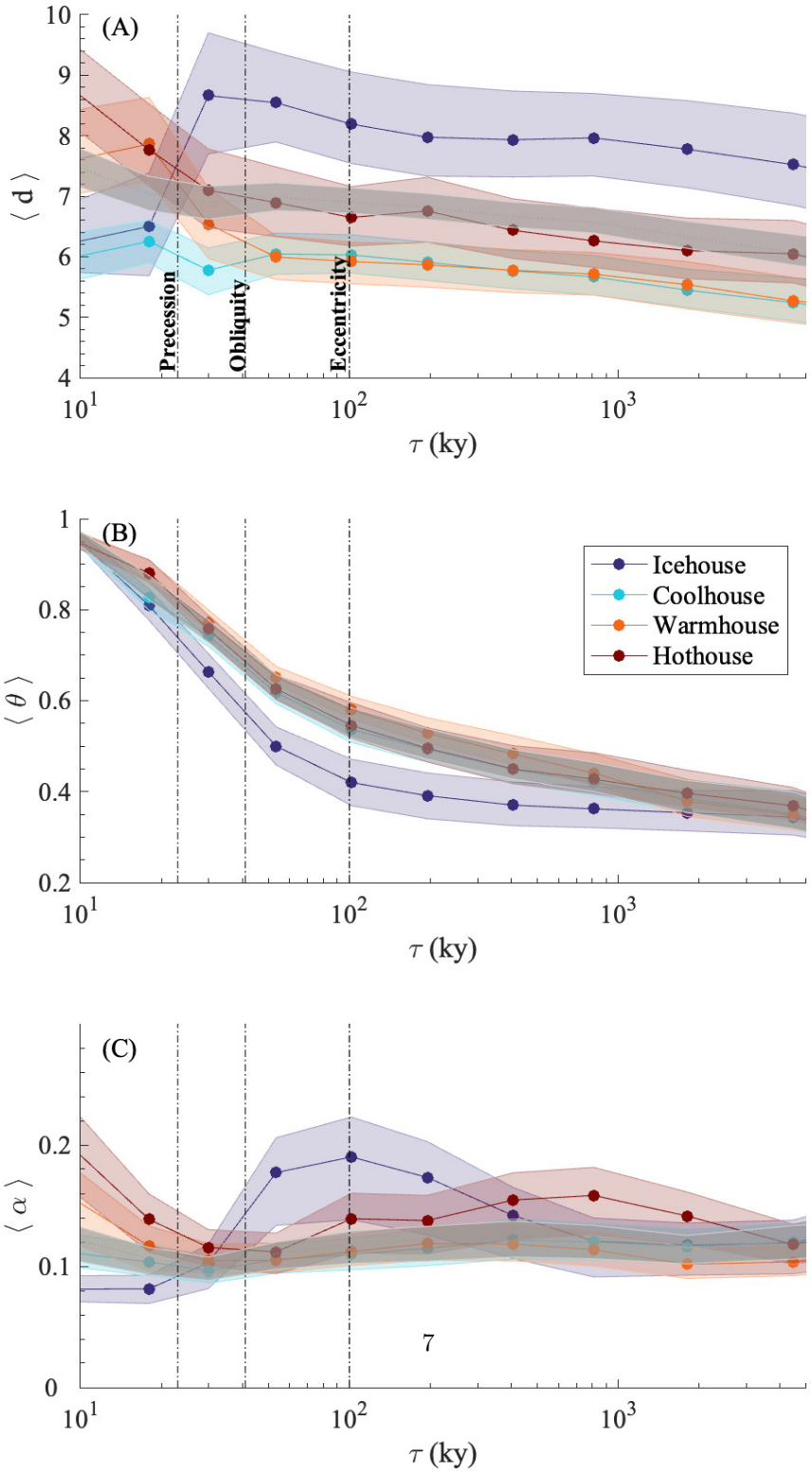

Fig. 3 Time-averaged multi-scale bi-variate statistics during the four climate states identified by [3]. Temporal averages of the bi-variate multi-scale metrics: (A) instantaneous dimension $\langle d \rangle$, (B) extremal index θ, and (C) co-recurrence ratio α. The error bars refers to the inter-quartile range. The vertical dashed-dotted black lines refer to Milankovitch scales of precession ($\sim$ 23 ky), obliquity ($\sim$ 41 ky), and eccentricity ($\sim$ 100 ky), respectively. Colors refer to the different climate states, while the gray shaded bars refer to the full record. We note that θ close to 0 (1) means a more (less) stable/persistent state, while α close to 0 (1) means a less (more) mutual coupling.

Figure S3) and in a uni-variate framework between two consecutive TPs identified by Rousseau et al. [18] (Supplementary Figures S4, S5).

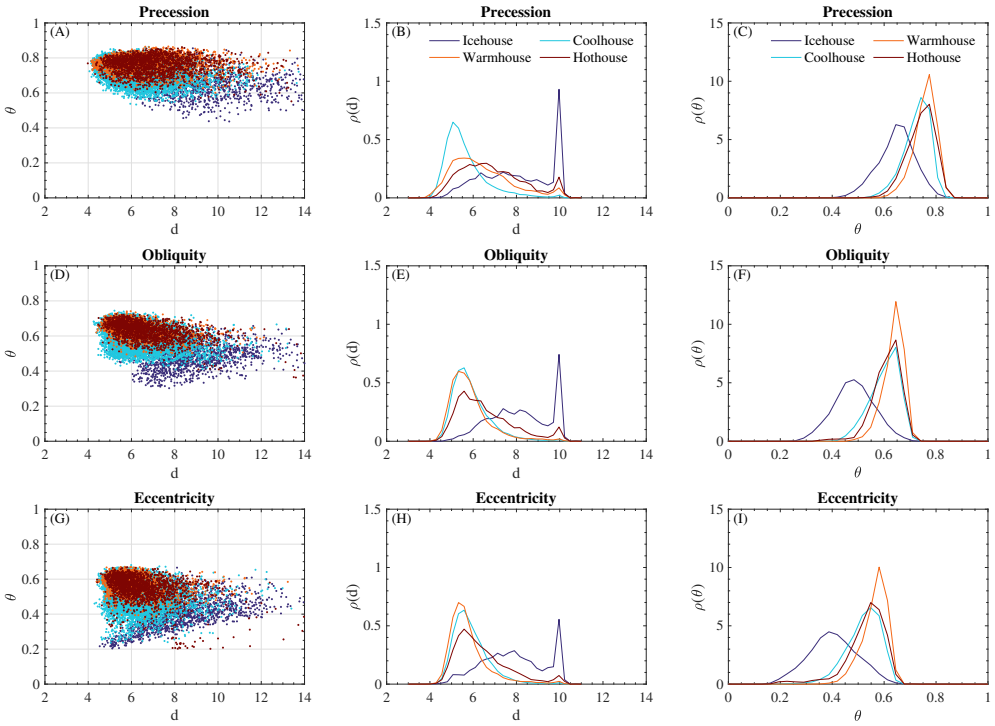

Fig. 4 Multiscale bivariate scatter-plots of the metrics at Milankovitch scales. $d - \theta$ scatter plots colored by time instants at the three Milankovitch scales of precession (A), obliquity (D), and eccentricity (G), respectively. The distribution of the instantaneous dimension d over the four different climate states identified by [3] at the three Milankovitch scales of precession (B), obliquity (E), and eccentricity (H), respectively. The distribution of the extremal index θ over the four different climate states identified by [3] at the three Milankovitch scales of precession (C), obliquity (F), and eccentricity (I), respectively. We remark that θ close to 0 (1) means more (less) stable/persistent state.

Moving across orbital timescales (Fig. 4 (A), (D), (G)) there is a transition toward a different portion of the 2-D parameter-space between warm (red and orange dots) and cold (cyan and violet dots) climates, which is particularly evident for the Icehouse (see violet dots in Fig. 4 (A)). Furthermore, for the Icehouse a wider spread in the range of values of both d (between 4 and 12) and θ (between 0.2 and 0.6) is observed at the eccentricity timescale, while a narrower θ-range occurs at the precession scale (between 0.5 and 0.7). A larger d range is seen during the part of the Coolhouse and the entire Icehouse; conversely, a confined region in the d-θ space (ranging d in 4-10 and θ in 0.65-0.85 or 0.55-0.75) is associated with both Hothouse and Warmhouse states. This is confirmed by the d and θ pdfs for the four climate states (Fig. 4 (B)-(C),

(E)-(F), (H)-(I)). The uniqueness of the Icehouse state is evidenced by the d distribution across orbital timescales which peaks at ∼10 for all Milankovitch cycles. The d distribution is also almost similar at all orbital timescales during the Coolhouse, albeit with a peak at lower values (∼5). Conversely, the two warm states are characterized by different d distributions across orbital timescales: a wider d spread occurs at the precession timescale, and more peaked distributions at obliquity and eccentricity timescales, which also shift toward lower values (∼5). The θ pdfs confirm the uniqueness of the Icehouse state: for all orbital timescales, θ is lower (more stable) during the Icehouse and the shape of the pdf is completely different relative to those of the other states, which turn are very similar to each other.

The unique nature of climate during the last ∼5 My is again evident from inspection of the dynamical properties of the Cenozoic climates compared with climates in different geological epochs with a similar bivariate approach (Supplementary Figure S3), as well as between two consecutive TPs of Rousseau et al. [18] using a uni-variate framework (Supplementary Figures S4, S5). Yes, our result is more pronounced in identifying the Icehouse as an unprecedented Cenozoic climate state. It is characterized by co-existence of widespread variability on two primary orbital timescales, through a large number of effective feedback mechanisms and with enhanced mutual coupling between atmosphere and ocean. In contrast, warmer climate states (Hothouse and Warmhouse) are characterized by a response at precession timescales, with relatively low average and instantaneous numbers of effective feedback mechanisms and low (Hothouse) to absent (Warmhouse) mutual coupling between δ^{13}C and δ^{18}O, apart from a high level of coupling during the exceptional PETM (mainly at timescales larger than the eccentricity period). The Coolhouse state is markedly different from both the warmer climate states and the Icehouse state, with low effective feedback mechanisms and coupling across timescales that lack a primary mode of variability for any orbital cycle. Our results enable interpretation of the time-evolution of Earth's Cenozoic climate system as a trajectory within a dynamic landscape that is characterized by multiscale features that delineate a hierarchy of metastable states and corresponding transitions.

Conclusions and Outlook

The Cenozoic era, spanning the last 66 million years, has witnessed significant changes in Earth's climate [3], including several diverse critical transitions [18]. Understanding the physical processes involved in this variability is crucial for interpreting paleoclimate data and projecting future climate scenarios [31]. Our analysis clearly highlights the crucial impact of polar ice sheet formation and evolution in regulating global climate, and feedback mechanisms have been critical to shaping these ice sheets. For example, polar ice sheet growth causes enhanced reflection of sunlight back into space, which causes further cooling that, in turn, fosters further ice growth (the positive ice-albedo feedback). Moreover, ice sheet waxing and waning is crucial in ocean-atmosphere coupling, which is at the basis of heat transport across the globe and thermal regulation of climate. And ice sheet fluctuations also affected vegetation-zone displacements, which further affect surface albedo and, thus, the energy balance of climate [32, 33].

We show here that the critical transitions identified in Ref. [18] are accompanied by anomalously large value in the number of effective feedback mechanisms and anomalously low values for the extremal index, which suggests dominant impacts of positive feedbacks. The instability in the extent of ice sheets during the Icehouse states is also associated with the anomalously high d values found in this period. In turn, our finding of an increased persistence (stability) of the Icehouse climate state agrees with a relatively stable Antarctic ice cover over extended periods despite varying climate conditions.

The climate responses to orbital forcing -which influences mainly the spatial and temporal distributions, and (weakly) the total amount of solar radiation reaching Earth's surface - consist of a complex interplay of positive and negative feedback. We find that positive feedback are more effective on specific orbital periods under different climate states. We detect that they acted on a dominant 23-ky (precession) timescale during Hothouse and Warmhouse climate states, mixed 41-ky (obliquity) and 100-ky (eccentricity) timescales during the Icehouse state, and that there is a remarkable lack of dominant timescales during the Coolhouse state. The detection of the primary variability timescales provides fundamental insights into the drivers of long-term climate variability and confirms the multiscale nature of climate variability [34, 35]. This is valuable information for understanding their significance in the context of future climate changes, and for assessing the capability of (paleo-)climate models to adequately replicate climate states and critical transitions between and within them. Crucially, our results suggest that there may be no unique model of interconnected feedback for reproducing paleoclimate variability across the entire Cenozoic era. Instead, we find that the different macro clusters of climate variability associated with the metastable states above are characterized by different numbers of feedback mechanisms that operate over different timescales for each climate state, and that this has considerable impacts on each climate state's inherent (in-)stability.

Methods

Empirical Mode Decomposition (EMD)

The Empirical Mode Decomposition (EMD) conforms with the class of adaptive decomposition methods and it allows us to decompose a time series $s(t)$ (e.g., δ^{13}C or δ^{18}O) into a finite number n_k of oscillating patterns $c_k(t)$, known as Intrinsic Mode Functions (IMFs), and a monotonic residue $r(t)$ as

$$s(t) = \sum_{k=1}^{n_k} c_k(t) + r(t). \tag{1}$$

The set of IMFs is derived via the so-called sifting process [25] which first identifies local extremes of $s(t)$ that are then interpolated via cubic splines to derive the upper and lower envelopes $u(t)$ and $\ell(t)$, respectively. Then, the mean envelope $m(t)$ is derived and the detail $h(t) = s(t) - m(t)$ is evaluated. If the detail $h(t)$ has the same (or differing by one) number of local extremes and zeros and a zero-average mean envelope, then the first IMF is obtained; otherwise, the steps of the sifting process

are iterated until these two properties are verified. The process stops when no more IMFs can be extracted and a monotonic non-oscillating function is obtained, i.e., the residue $r(t)$.

The EMD provides a representation of the system as a sum of fluctuating contributions at different average timescales [25], although each of them is a non-stationary function with a time-dependent amplitude and phase, i.e., $c_k(t) = a_k(t)\cos[\phi_k(t)]$. The instantaneous amplitude $a_k(t)$ and phase $\phi_k(t)$ are derived via the Hilbert transform. The reader is referred to [25] for further detail.

Uni-variate metrics

Instantaneous dimension

In a system described by the time-evolution of a given variable, i.e., via a time series $s(t)$, each time instant can be seen as a *state* of the system that can eventually be visited several times in the future, and whose dynamical properties can be investigated by combining recurrence and extreme value theory [36]. For any given state of interest ζ, the logarithmic return of each state except ζ is

$$g(t) = -\log\left[\delta(s(t), \zeta)\right] \tag{2}$$

where δ is the Euclidean distance between two state vectors. As $s(t)$ approaches ζ then $g(t)$ goes to infinite. If we define a threshold $s(q)$ as the q-th empirical quantile of $g(t)$, we can introduce the exceedances $u(\zeta) \doteq \{t \,|\, g(t) > s(q)\}$, which represent the occurrences that exceed the neighborhood of the reference state. This concept was first introduced by Poincaré [37] and is akin to the peaks-over-threshold approach widely used in extreme value theory. According to the Freitas-Freitas-Todd theorem [38], the cumulative probability distribution $F(u, \zeta)$ then converges to the exponential member of the Generalised Pareto Distribution (GPD), expressed as follows:

$$F(u, \zeta) \simeq \exp\left[-\frac{u(\zeta)}{\varsigma(\zeta)}\right]. \tag{3}$$

The GPD parameter ς depends on the dynamical state ζ and can be used to introduce the concept of an instantaneous dimension d at the point in time where ζ is attained. This instantaneous dimension is simply defined as $d(\zeta) = \varsigma(\zeta)^{-1}$ and represents a proxy for the number of active feedback determining the behavior of the system around each state ζ in the phase-space [26, 27, 36, 39]. However, it is essential to note that from a practical perspective, this instantaneous dimension needs to be considered relative to the set of time series values available and also to be understood in a relative sense. Indeed, averaging over the phase-space gives an estimation of the information dimension of the system, i.e., how much space the system explores and how intricate its patterns are, while the gradient (increase or decrease) of the instantaneous dimension indicates structures which feature more or less feedback mechanisms.

Extremal index

The Süveges maximum likelihood estimator is used for evaluating the extremal index [40, 41], which provides information on the time spent by the system in a given state ζ:

$$\theta = \frac{\sum_{i=1}^{N} \rho S_i + N - 1 + N_c - \left[\left(\sum_{i=1}^{N-1} \rho S_i + N - 1 + N_c\right)^2 - 8N_c \sum_{i=1}^{N-1} \rho S_i\right]^{1/2}}{2\sum_{i=1}^{N-1} \rho S_i}. \quad (4)$$

Here, N represents the number of observations exceeding a defined threshold, ρ is the distribution function of the selected threshold, S_i denotes the exceeding distance, and $N_c = \sum_{i=1}^{N-1} I(S_i \neq 0)$, where I is the indicator function for the selected S_i. Further details on the calculation can be found in [40]. The extremal index θ can be introduced in Eq. (3) as follows:

$$F(u, \zeta) \simeq \exp\left[-\theta(\zeta)\,\frac{u(\zeta)}{\varsigma(\zeta)}\right]. \quad (5)$$

As $\theta(\zeta) \in [0, 1]$, the state ζ is more persistent as $\theta(\zeta) \to 0$, whereas when $\theta(\zeta) \to 1$, the state ζ is unstable, and the system immediately leaves ζ [27, 41]. An exploration of all states (i.e., all time instants) provides an instantaneous view of the persistence of the system into different states. Consequently, each state ζ of the system, corresponding to the time instant t of the time series, is now described by the pair (d, θ). These metrics have offered fresh insights and a different perspective on various geophysical extreme phenomena [42–49].

Bi-variate metrics

The two metrics presented before enable us to retain information about a given system within a *uni-variate* framework, i.e., as described via a single variable $s(t)$. We can extend this formalism to the *bi-variate* case by considering a system described by a pair of variables, i.e., $x(t)$ and $y(t)$. If we define their associated reference state as $\zeta = \{\zeta_x, \zeta_y\}$, the joint logarithmic return is

$$g(x, y; \zeta) = -\frac{1}{2}\log\left[\delta(x(t), \zeta_x)^2 + \delta(y(t), \zeta_y)^2\right]. \quad (6)$$

As for the uni-variate case we can compute the *co-dimension* d_{xy}, representing the mutual number of feedback given by x and y in terms of their joint recurrences, or in other words implying that a given reference state ζ is simultaneously observed in both variables. similarly, the bi-variate extremal index θ_{xy} can be defined as a weighted average of θ_x and θ_y [50].

In the bi-variate framework an additional dynamical system metric can be introduced that provides a measure of the mutual coupling between x and y. It is known as the co-recurrence ratio α

$$\alpha = \frac{\#\left[g(\mathbf{x}; \zeta_x) > g_q(\mathbf{x}; \zeta_x) | g(\mathbf{y}; \zeta_y) > g_q(\mathbf{y}; \zeta_y)\right]}{\#\left[g(\mathbf{x}; \zeta_x) > g_q(\mathbf{x}; \zeta_x)\right]}, \quad (7)$$

where $\#[\cdot]$ denotes the number of events satisfying the condition $[\cdot]$. It measures the percentage of states ζ for which x resembles ζ_x, given that y resembles ζ_y. If $\alpha = 0$, there are no mutual co-recurrences; if $\alpha = 1$ then a stronger coupling is present between x and y. However, due to the Bayesian formulation of Eq. (7) α cannot be interpreted in terms of causation but only as a measure of mutual relation between the variables [50].

Instantaneous scale-dependent metrics

The previous discussion introduced the concepts of instantaneous dimension d and inverse persistence θ to provide a local view of phase-space trajectory properties. This allows us to obtain information for each sampled point contributing to the global structure of the phase-space under study. However, in the case of multi-scale systems characterized by processes occurring over a wide range of scales, a scale-dependent phase-space structure can emerge [51]. To obtain a scale-dependent instantaneous view of such systems, a combination of the Empirical Mode Decomposition (EMD) method and extreme value theory is used.

For a multi-scale system described by $s(t)$, we can express it as:

$$s(t) = \langle s(t) \rangle + \sum_{\tau} \delta s^{(\tau)}(t), \tag{8}$$

where $\langle s(t) \rangle$ represents a steady-state time-averaged value, and $\delta s^{(\tau)}(t)$ is a component of the system operating at a mean scale τ. An analogy can be drawn between Eq. (8) and Eq. (1) with the correspondence $c_k(t) \leftrightarrow \delta s^{(\tau)}(t)$ and $r(t) \leftrightarrow \langle s(t) \rangle$. This means that for each scale τ, we can identify the corresponding invariant set $M\tau$ as the manifold obtained via the partial sums of Intrinsic Mode Functions (IMFs) with scales $\tau\star < \tau$:

$$s^{\tau}(t) = \sum_{k^{\star}=1}^{k} c_{k^{\star}}(t), \tag{9}$$

For each scale $\tau \in [\tau_1, \tau_{n_k}]$, where n_k is the number of IMFs, given a trajectory $s^{\tau}(t)$ and a state of interest ζ_{τ}, the cumulative probability of logarithmic returns in the neighborhood of ζ_{τ} follows a Generalized Pareto Distribution (GPD):

$$F(u_{\tau}, \zeta_{\tau}) \simeq \exp\left[-\theta_{\tau}(\zeta_{\tau}), \frac{u_{\tau}(\zeta_{\tau})}{\varsigma_{\tau}(\zeta_{\tau})}\right]. \tag{10}$$

Thus, two scale-dependent metrics $d(t, \tau) = \varsigma_{\tau}(\zeta_{\tau})^{-1}$ and $\theta(t, \tau)$ can be introduced, representing the number of active feedback and the stability/persistence of fluctuations up to a maximum scale of τ around each state ζ_{τ}. In a similar fashion we can introduce, in a bi-variate framework, the scale-dependent co-recurrent ratio $\alpha(t, \tau)$. By using the EMD to derive scale-dependent components within the system and extreme value theory-based metrics to obtain the instantaneous scale-dependent metrics, this approach provides valuable insights into the system's behavior at different scales [23, 24].

Data Availability

All data are available open access in electronic form at the PANGAEA data repository (https://doi.org/10.1594/PANGAEA.917503).

Code Availability

The code to perform the analogues dynamical analysis is available at https://fr.mathworks.com/matlabcentral/fileexchange/95768-attractor-local-dimension-and-local-persistence-computation.

Acknowledgments

V.L. acknowledges the support received from the EPSRC project EP/T018178/1 and from the EU Horizon 2020 project TiPES (Grant no. 820970).

Competing Interest

The authors declare no competing interests nor conflicts of interest. No human or animal data have been used in this study.

Author Contributions

TA and FF designed research, TA, EJR, and VL performed research, TA and DF analyzed data. All authors contributed to discussing and writing the paper.

Declarations

The authors declare no conflict of interests.

References

[1] Savin, S.M., Douglas, R.G., Stehli, F.G.: Tertiary marine paleotemperatures. Geological Society of America Bulletin **86**(11), 1499 (1975) https://doi.org/10.1130/0016-7606(1975)86⟨1499:TMP⟩2.0.CO;2

[2] Kennett, J.P., Shackleton, N.J.: Laurentide Ice Sheet Meltwater Recorded in Gulf of Mexico Deep-Sea Cores. Science **188**(4184), 147–150 (1975) https://doi.org/10.1126/science.188.4184.147

[3] Westerhold, T., Marwan, N., Drury, A.J., Liebrand, D., Agnini, C., Anagnostou, E., Barnet, J.S.K., Bohaty, S.M., De Vleeschouwer, D., Florindo, F., Frederichs, T., Hodell, D.A., Holbourn, A.E., Kroon, D., Lauretano, V., Littler, K., Lourens, L.J., Lyle, M., Pälike, H., Röhl, U., Tian, J., Wilkens, R.H., Wilson, P.A., Zachos, J.C.: An astronomically dated record of Earth's climate and its predictability

over the last 66 million years. Science **369**(6509), 1383–1387 (2020) https://doi.org/10.1126/science.aba6853

[4] Lourens, L.J., Sluijs, A., Kroon, D., Zachos, J.C., Thomas, E., Röhl, U., Bowles, J., Raffi, I.: Astronomical pacing of late Palaeocene to early Eocene global warming events. Nature **435**(7045), 1083–1087 (2005) https://doi.org/10.1038/nature03814

[5] Nicolo, M.J., Dickens, G.R., Hollis, C.J., Zachos, J.C.: Multiple early Eocene hyperthermals: Their sedimentary expression on the New Zealand continental margin and in the deep sea. Geology **35**(8), 699 (2007) https://doi.org/10.1130/G23648A.1

[6] Zachos, J.C., McCarren, H., Murphy, B., Röhl, U., Westerhold, T.: Tempo and scale of late Paleocene and early Eocene carbon isotope cycles: Implications for the origin of hyperthermals. Earth and Planetary Science Letters **299**(1-2), 242–249 (2010) https://doi.org/10.1016/j.epsl.2010.09.004

[7] Gutjahr, M., Ridgwell, A., Sexton, P.F., Anagnostou, E., Pearson, P.N., Pälike, H., Norris, R.D., Thomas, E., Foster, G.L.: Very large release of mostly volcanic carbon during the Palaeocene-Eocene Thermal Maximum. Nature **548**(7669), 573–577 (2017) https://doi.org/10.1038/nature23646

[8] Galeotti, S., DeConto, R., Naish, T., Stocchi, P., Florindo, F., Pagani, M., Barrett, P., Bohaty, S.M., Lanci, L., Pollard, D., Sandroni, S., Talarico, F.M., Zachos, J.C.: Antarctic Ice Sheet variability across the Eocene-Oligocene boundary climate transition. Science **352**(6281), 76–80 (2016) https://doi.org/10.1126/science.aab0669

[9] Coxall, H.K., Wilson, P.A., Pälike, H., Lear, C.H., Backman, J.: Rapid stepwise onset of Antarctic glaciation and deeper calcite compensation in the Pacific Ocean. Nature **433**(7021), 53–57 (2005) https://doi.org/10.1038/nature03135

[10] Scher, H.D., Bohaty, S.M., Zachos, J.C., Delaney, M.L.: Two-stepping into the icehouse: East Antarctic weathering during progressive ice-sheet expansion at the Eocene-Oligocene transition. Geology **39**(4), 383–386 (2011) https://doi.org/10.1130/G31726.1

[11] Barr, I.D., Spagnolo, M., Rea, B.R., Bingham, R.G., Oien, R.P., Adamson, K., Ely, J.C., Mullan, D.J., Pellitero, R., Tomkins, M.D.: 60 million years of glaciation in the Transantarctic Mountains. Nature Communications **13**, 5526 (2022) https://doi.org/10.1038/s41467-022-33310-z

[12] Rohling, E.J., Foster, G.L., Gernon, T.M., Grant, K.M., Heslop, D., Hibbert, F.D., Roberts, A.P., Yu, J.: Comparison and Synthesis of Sea-Level and Deep-Sea Temperature Variations Over the Past 40 Million Years. Reviews of Geophysics **60**(4), 2022–000775 (2022) https://doi.org/10.1029/2022RG000775

[13] Flower, B.P., Kennett, J.P.: The middle Miocene climatic transition: East Antarctic ice sheet development, deep ocean circulation and global carbon cycling. Palaeogeography Palaeoclimatology Palaeoecology **108**(3-4), 537–555 (1994) https://doi.org/10.1016/0031-0182(94)90251-8

[14] Raitzsch, M., Bijma, J., Bickert, T., Schulz, M., Holbourn, A., Kučera, M.: Atmospheric carbon dioxide variations across the middle Miocene climate transition. Climate of the Past **17**(2), 703–719 (2021) https://doi.org/10.5194/cp-17-703-2021

[15] Bailey, I., Hole, G.M., Foster, G.L., Wilson, P.A., Storey, C.D., Trueman, C.N., Raymo, M.E.: An alternative suggestion for the Pliocene onset of major northern hemisphere glaciation based on the geochemical provenance of North Atlantic Ocean ice-rafted debris. Quaternary Science Reviews **75**, 181–194 (2013) https://doi.org/10.1016/j.quascirev.2013.06.004

[16] Zachos, J., Pagani, M., Sloan, L., Thomas, E., Billups, K.: Trends, rhythms, and aberrations in global climate 65 ma to present. Science **292**(5517), 686–693 (2001) https://doi.org/10.1126/science.1059412 https://www.science.org/doi/pdf/10.1126/science.1059412

[17] Lenton, T.M., Held, H., Kriegler, E., Hall, J.W., Lucht, W., Rahmstorf, S., Schellnhuber, H.J.: Tipping elements in the earth's climate system. Proceedings of the National Academy of Sciences **105**(6), 1786–1793 (2008) https://doi.org/10.1073/pnas.0705414105 https://www.pnas.org/doi/pdf/10.1073/pnas.0705414105

[18] Rousseau, D.-D., Bagniewski, W., Lucarini, V.: A punctuated equilibrium analysis of the climate evolution of cenozoic exhibits a hierarchy of abrupt transitions. Scientific Reports **13**, 11290 (2023) https://doi.org/10.1038/s41598-023-38454-6 arXiv:2212.06239 [physics.ao-ph]

[19] Marwan, N., Carmen Romano, M., Thiel, M., Kurths, J.: Recurrence plots for the analysis of complex systems. Physics Reports **438**(5), 237–329 (2007) https://doi.org/10.1016/j.physrep.2006.11.001

[20] Bagniewski, W., Rousseau, D.-D., Ghil, M.: The paleojump database for abrupt transitions in past climates. Scientific Reports **13**(1), 4472 (2023) https://doi.org/10.1038/s41598-023-30592-1

[21] Lucarini, V., Bodai, T.: Global stability properties of the climate: Melancholia states, invariant measures, and phase transitions. Nonlinearity **33**(9), 59 (2020) https://doi.org/10.1088/1361-6544/ab86cc

[22] Margazoglou, G., Grafke, T., Laio, A., Lucarini, V.: Dynamical landscape and multistability of a climate model. Proceedings of the Royal Society A: Mathematical, Physical and Engineering Sciences

477(2250), 20210019 (2021) https://doi.org/10.1098/rspa.2021.0019 https://royalsocietypublishing.org/doi/pdf/10.1098/rspa.2021.0019

[23] Alberti, T., Faranda, D., Lucarini, V., Donner, R.V., Dubrulle, B., Daviaud, F.: Scale dependence of fractal dimension in deterministic and stochastic Lorenz-63 systems. Chaos **33**(2), 023144 (2023) https://doi.org/10.1063/5.0106053 arXiv:2206.13154 [nlin.CD]

[24] Alberti, T., Daviaud, F., Donner, R.V., Dubrulle, B., Faranda, D., Lucarini, V.: Chameleon attractors in turbulent flows. Chaos Solitons and Fractals **168**, 113195 (2023) https://doi.org/10.1016/j.chaos.2023.113195

[25] Huang, N.E., Shen, Z., Long, S.R., Wu, M.C., Shih, H.H., Zheng, Q., Yen, N.-C., Tung, C.C., Liu, H.H.: The empirical mode decomposition and the Hilbert spectrum for nonlinear and non-stationary time series analysis. Proceedings of the Royal Society of London Series A **454**(1971), 903–998 (1998) https://doi.org/10.1098/rspa.1998.0193

[26] Lucarini, V.: Stochastic perturbations to dynamical systems: A response theory approach. Journal of Statistical Physics **146**(4), 774–786 (2012) https://doi.org/10.1007/s10955-012-0422-0

[27] Lucarini, V., Faranda, D., Freitas, A.C.G.M.M., Freitas, J.M.M., Holland, M., Kuna, T., Nicol, M., Todd, M., Vaienti, S.: Extremes and Recurrence in Dynamical Systems. Wiley, New York (2016)

[28] Faranda, D., Messori, G., Yiou, P.: Dynamical proxies of North Atlantic predictability and extremes. Scientific Reports **7**, 41278 (2017) https://doi.org/10.1038/srep41278

[29] Arnscheidt, C.W., Rothman, D.H.: Presence or absence of stabilizing earth system feedbacks on different time scales. Science Advances **8**(46), 9241 (2022) https://doi.org/10.1126/sciadv.adc9241 https://www.science.org/doi/pdf/10.1126/sciadv.adc9241

[30] Sosdian, S.M., Babila, T.L., Greenop, R., Foster, G.L., Lear, C.H.: Ocean Carbon Storage across the middle Miocene: a new interpretation for the Monterey Event. Nature Communications **11**, 134 (2020) https://doi.org/10.1038/s41467-019-13792-0

[31] IPCC: Climate Change 2022: Mitigation of Climate Change. Contribution of Working Group III to the Sixth Assessment Report of the Intergovernmental Panel on Climate Change. Cambridge University Press, Cambridge, UK and New York, NY, USA (2022). https://doi.org/10.1017/9781009157926

[32] Alberti, T., Primavera, L., Vecchio, A., Lepreti, F., Carbone, V.: Spatial interactions in a modified Daisyworld model: Heat diffusivity and greenhouse effects.

Phys. Rev E **92**(5), 052717 (2015) https://doi.org/10.1103/PhysRevE.92.052717

[33] Rombouts, J., Ghil, M.: Oscillations in a simple climate-vegetation model. Nonlinear Processes in Geophysics **22**(3), 275–288 (2015) https://doi.org/10.5194/npg-22-275-201510.5194/npgd-2-145-2015

[34] Ghil, M., Lucarini, V.: The physics of climate variability and climate change. Reviews of Modern Physics **92**(3), 035002 (2020) https://doi.org/10.1103/RevModPhys.92.035002 arXiv:1910.00583 [physics.ao-ph]

[35] von der Heydt, A.S., Ashwin, P., Camp, C.D., Crucifix, M., Dijkstra, H.A., Ditlevsen, P., Lenton, T.M.: Quantification and interpretation of the climate variability record. Global and Planetary Change **197**, 103399 (2021) https://doi.org/10.1016/j.gloplacha.2020.103399

[36] Lucarini, V., Faranda, D., Turchetti, G., Vaienti, S.: Extreme value theory for singular measures. Chaos **22**(2), 023135 (2012) https://doi.org/10.1063/1.4718935

[37] Poincaré, H.: Sur le problème des trois corps et les équations de la dynamique. Acta mathematica **13**(1), 3–270 (1890)

[38] Freitas, A.C.M., Freitas, J.M., Todd, M.: Extreme Value Laws in Dynamical Systems for Non-smooth Observations. Journal of Statistical Physics **142**(1), 108–126 (2011) https://doi.org/10.1007/s10955-010-0096-4

[39] Lucarini, V., Faranda, D., Wouters, J., Kuna, T.: Towards a General Theory of Extremes for Observables of Chaotic Dynamical Systems. Journal of Statistical Physics **154**(3), 723–750 (2014) https://doi.org/10.1007/s10955-013-0914-6 arXiv:1301.0733 [cond-mat.stat-mech]

[40] Süveges, M.: Likelihood estimation of the extremal index. Extremes **10**(1-2), 41–55 (2007) https://doi.org/10.1007/s10687-007-0034-2

[41] Moloney, N.R., Faranda, D., Sato, Y.: An overview of the extremal index. Chaos **29**(2), 022101 (2019) https://doi.org/10.1063/1.5079656

[42] Faranda, D., Alvarez-Castro, M.C., Messori, G., Rodrigues, D., Yiou, P.: The hammam effect or how a warm ocean enhances large scale atmospheric predictability. Nature communications **10**(1), 1–7 (2019)

[43] De Luca, P., Messori, G., Faranda, D., Ward, P.J., Coumou, D.: Compound warm–dry and cold–wet events over the mediterranean. Earth System Dynamics **11**(3), 793–805 (2020)

[44] Faranda, D., Vrac, M., Yiou, P., Jézéquel, A., Thao, S.: Changes in future synoptic circulation patterns: consequences for extreme event attribution. Geophysical

Research Letters **47**(15), 2020–088002 (2020)

[45] Faranda, D., Messori, G., Yiou, P.: Diagnosing concurrent drivers of weather extremes: application to warm and cold days in north america. Climate Dynamics **54**(3), 2187–2201 (2020)

[46] Alberti, T., Faranda, D., Consolini, G., De Michelis, P., Donner, R.V., Carbone, V.: Concurrent effects between geomagnetic storms and magnetospheric substorms. Universe **8**(4), 226 (2022)

[47] Gualandi, A., Avouac, J.-P., Michel, S., Faranda, D.: The predictable chaos of slow earthquakes. Science advances **6**(27), 5548 (2020)

[48] Alberti, T., De Michelis, P., Santarelli, L., Faranda, D., Consolini, G., Marcucci, M.F.: Tracking Geomagnetic Storms with Dynamical System Approach: Ground-Based Observations. Remote Sensing **15**(12), 3031 (2023) https://doi.org/10.3390/rs15123031

[49] Alberti, T., Anzidei, M., Faranda, D., Vecchio, A., Favaro, M., Papa, A.: Dynamical diagnostic of extreme events in Venice lagoon and their mitigation with the MoSE. Scientific Reports **13**, 10475 (2023) https://doi.org/10.1038/s41598-023-36816-8

[50] Faranda, D., Messori, G., Yiou, P.: Diagnosing concurrent drivers of weather extremes: application to warm and cold days in North America. Climate Dynamics **54**(3-4), 2187–2201 (2020) https://doi.org/10.1007/s00382-019-05106-3

[51] Alberti, T., Consolini, G., Ditlevsen, P.D., Donner, R.V., Quattrociocchi, V.: Multiscale measures of phase-space trajectories. Chaos **30**(12), 123116 (2020) https://doi.org/10.1063/5.0008916